Supporting Information for

Low-Cost and Sustainable Hard Carbon Derived from the Peony Shell for the Stable Sodium-Ion Anode

Haopo Li, Fang Wang,* Zhangqin Shi, Fangya Guo, Ting Feng, Huimin Han, Nuoyan Wang, Shuaisong Wang, Yuting Yang, Haitao Wu, Yi Xiong, Fengzhang Ren,* Xinyang Yue*

*Corresponding authors:
wangfang1116@163.com (F.W.)
renfz@haust.edu.cn (F.R.)
xinyangyue@sjtu.edu.cn (X.Y.)

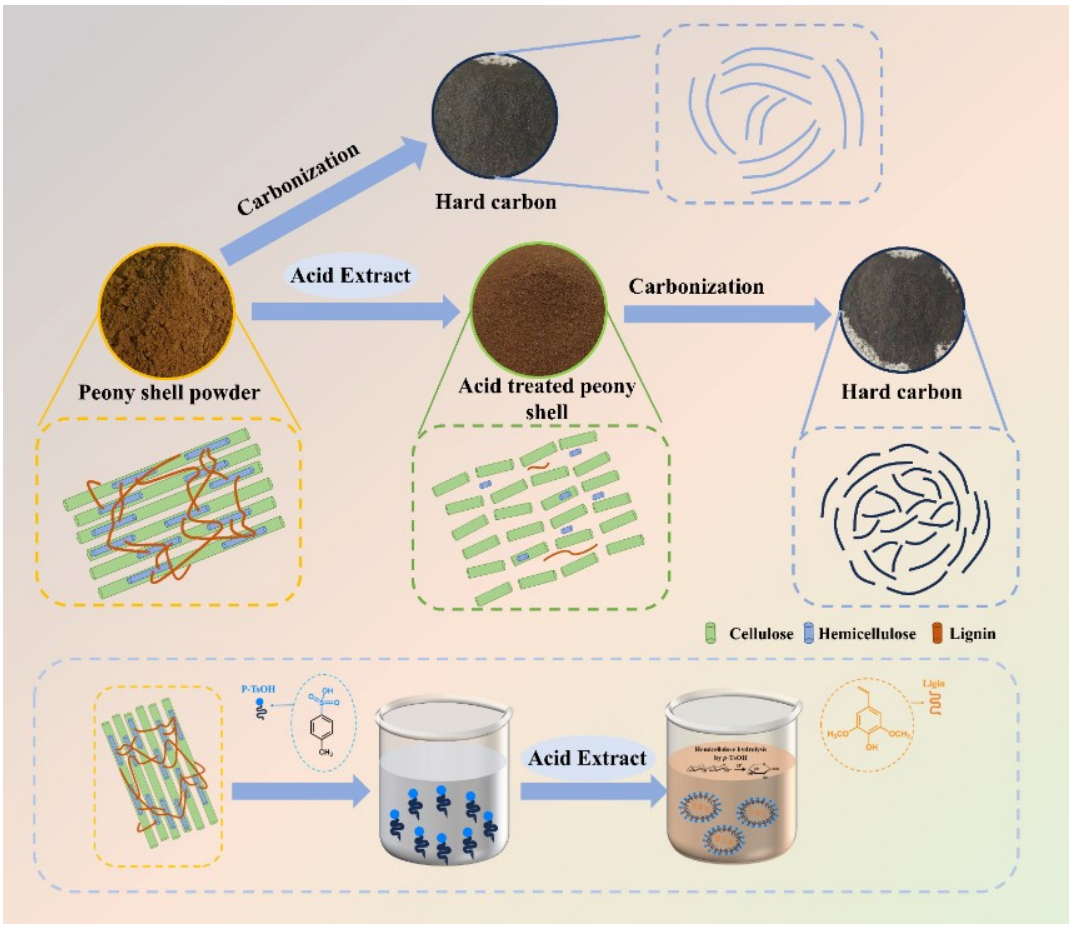

Fig. S1. Schematic of the preparation process for HC materials.

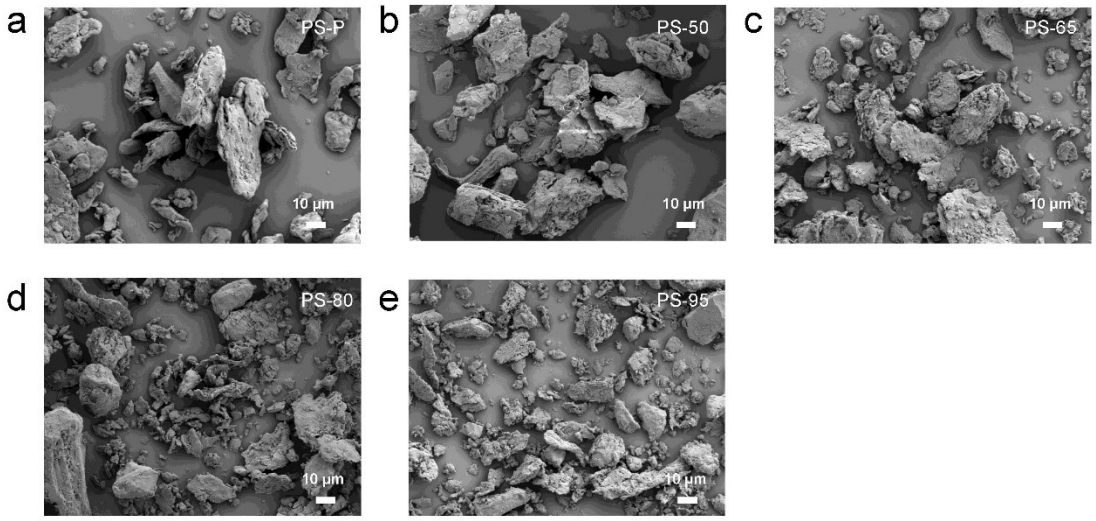

Fig. S2. SEM images of (a) PS-P, (b) PS-50, (c) PS-65, (d) PS-80, and (e) PS-95.

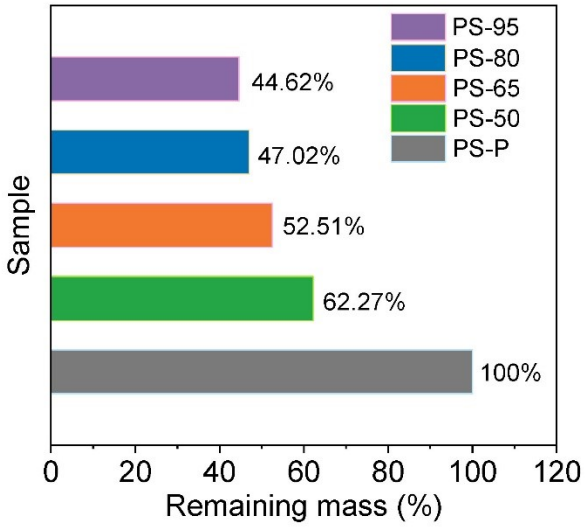

Fig. S3. Quality residual diagram after acid treatment.

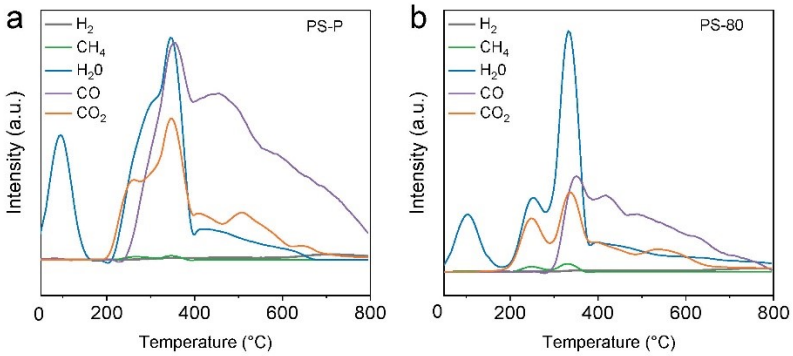

Fig. S4. MS results of (a) PHC-T0 and (b) PHC-T80.

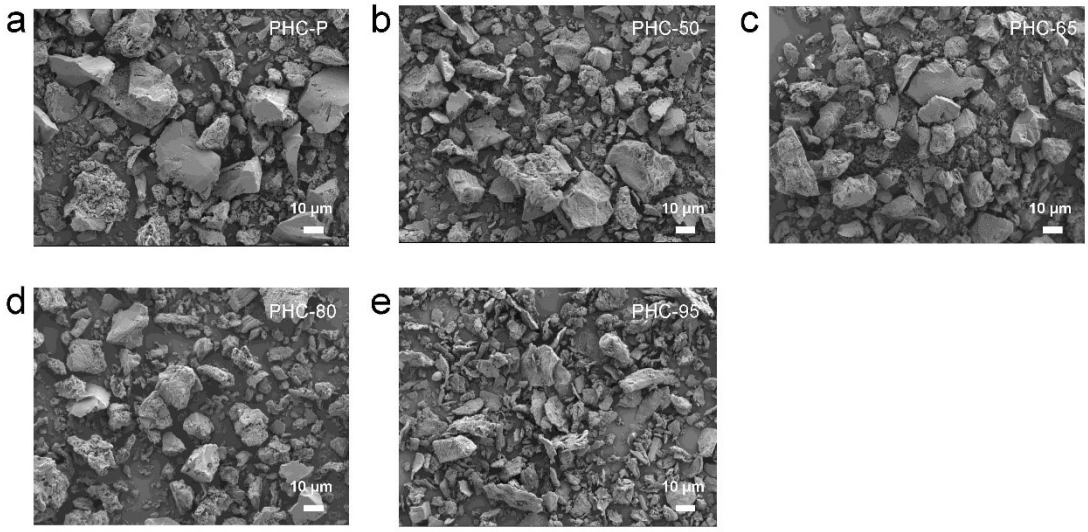

Fig. S5. SEM images of (a) PHC-P, (b) PHC-50, (c) PHC-65, (d) PHC-80, and (e) PHC-95.

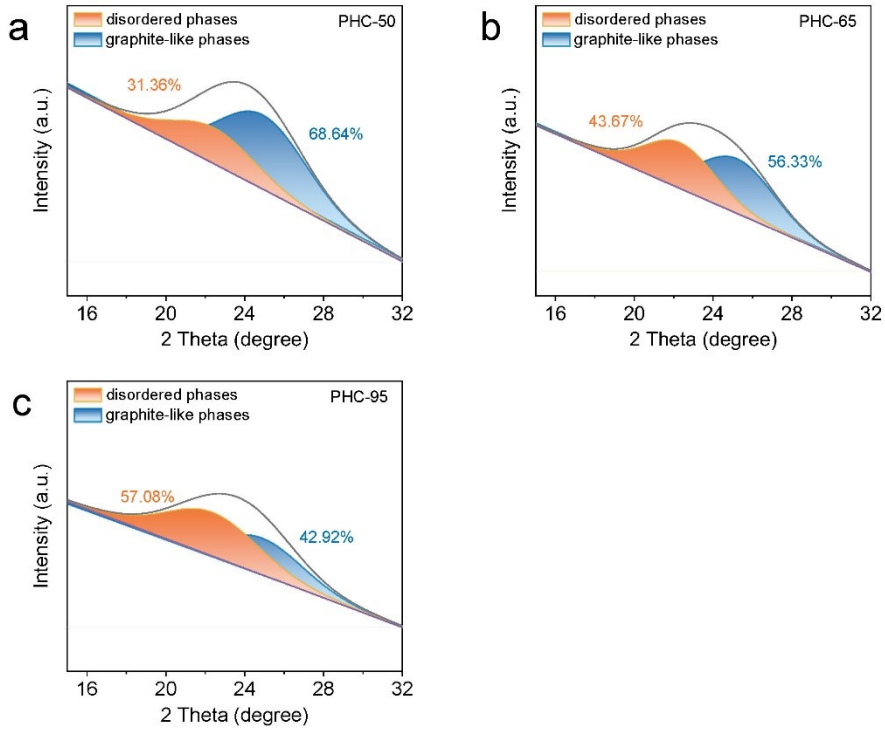

Fig. S6. XRD patterns and fitted curves of (a) PHC-50, (b) PHC-65, and (c) PHC-95.

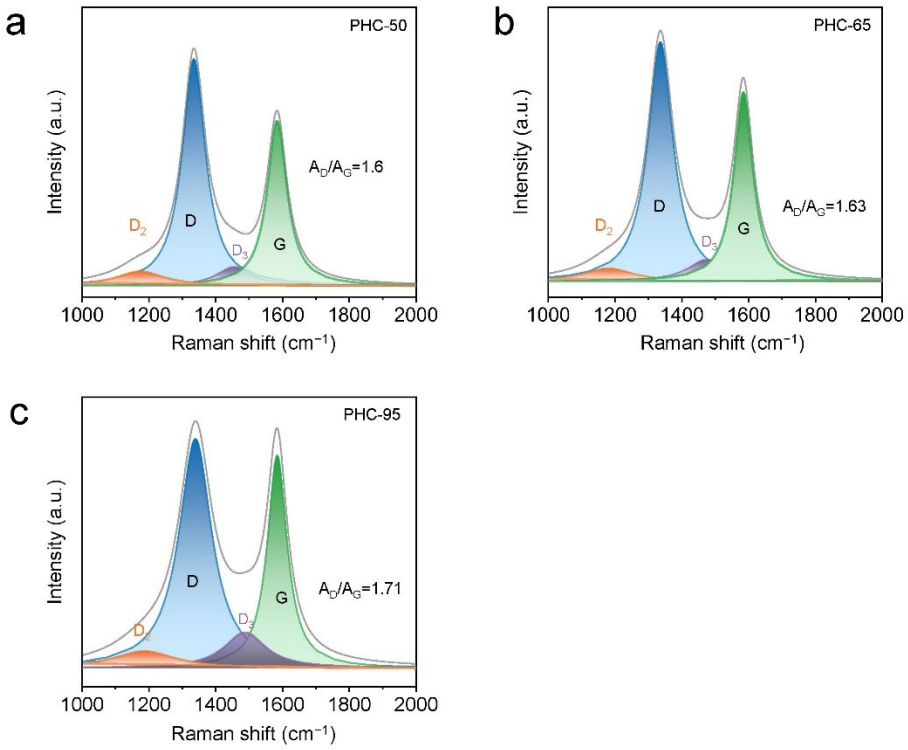

Fig. S7. Raman patterns and fitted curves of (a) PHC-50, (b) PHC-65, and (c) PHC-95.

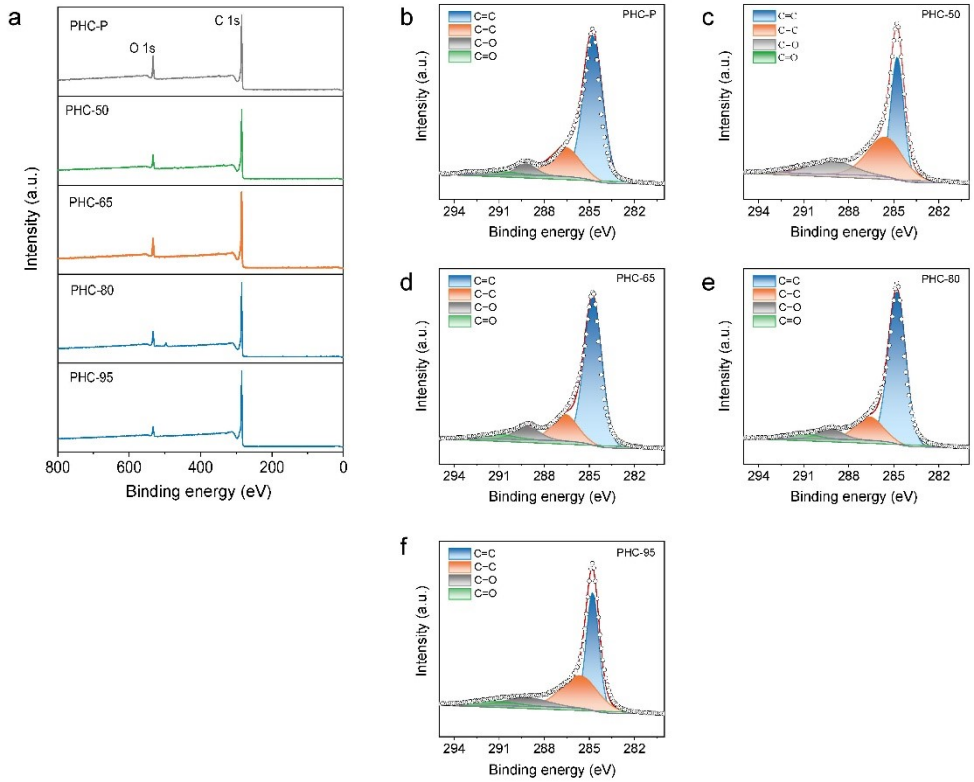

Fig. S8. (a) XPS pattern of samples. XPS C 1s spectra of (b) PHC-P, (c) PHC-50, (d) PHC-65, (e) PHC-80, and (f) PHC-95.

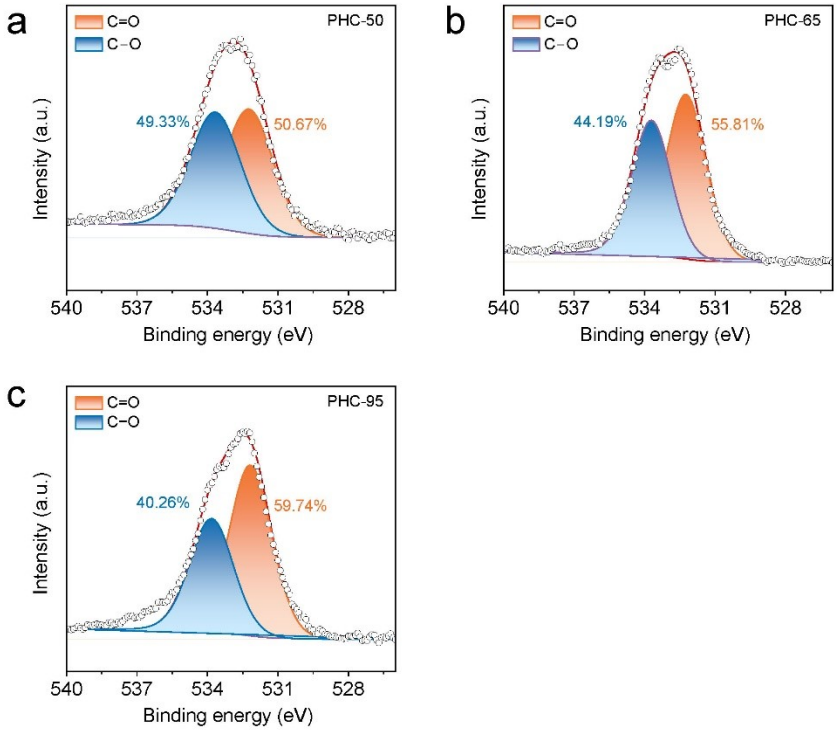

Fig. S9. XPS patterns and fitted curves of (a) PHC-50, (b) PHC-65, and (c) PHC-95.

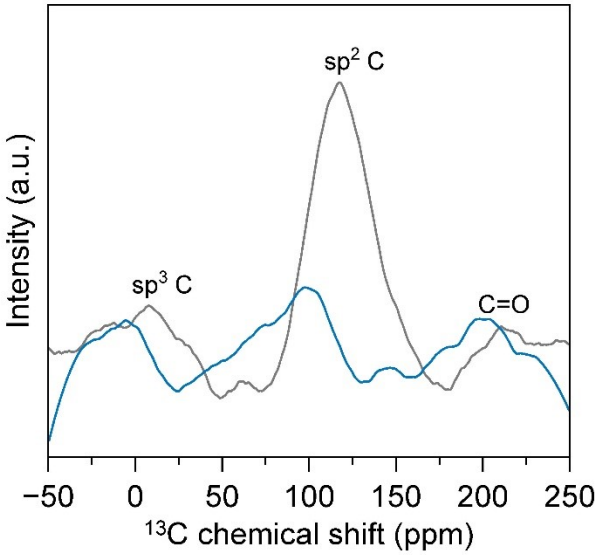

Fig. S10. ^{13}C NMR spectra of PHC-P and PHC-80.

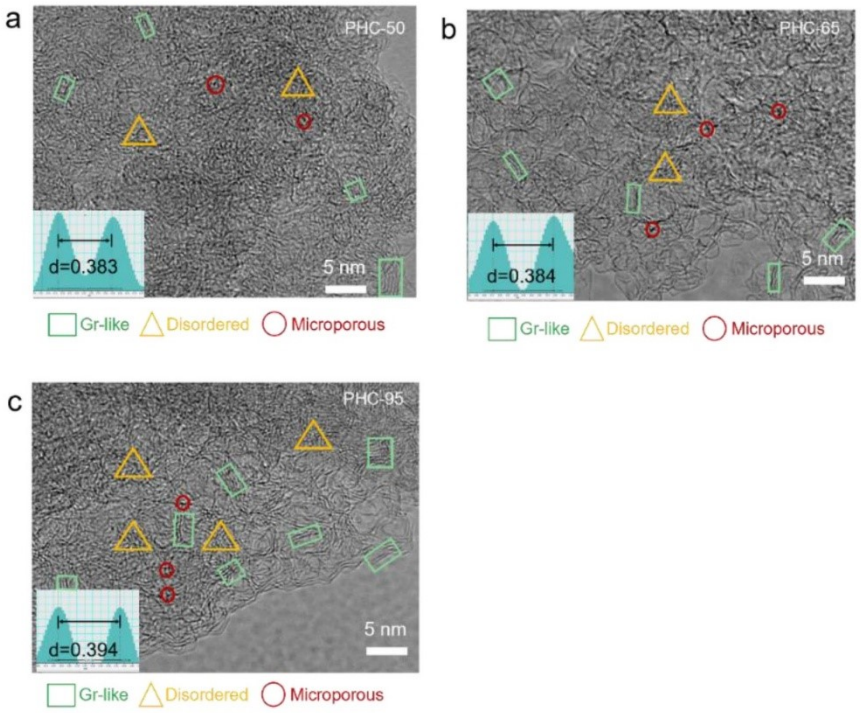

Fig. S11. TEM images of (a) PHC-50, (b) PHC-65, and (c) PHC-95.

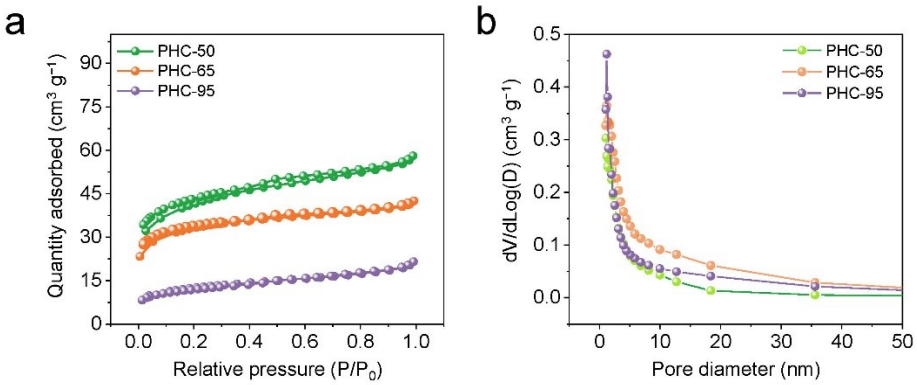

Fig. S12. (a) N_2 adsorption-desorption isotherms and (b) pore size distribution of N_2 adsorption-desorption isotherms of PHC-50, PHC-65, and PHC-95.

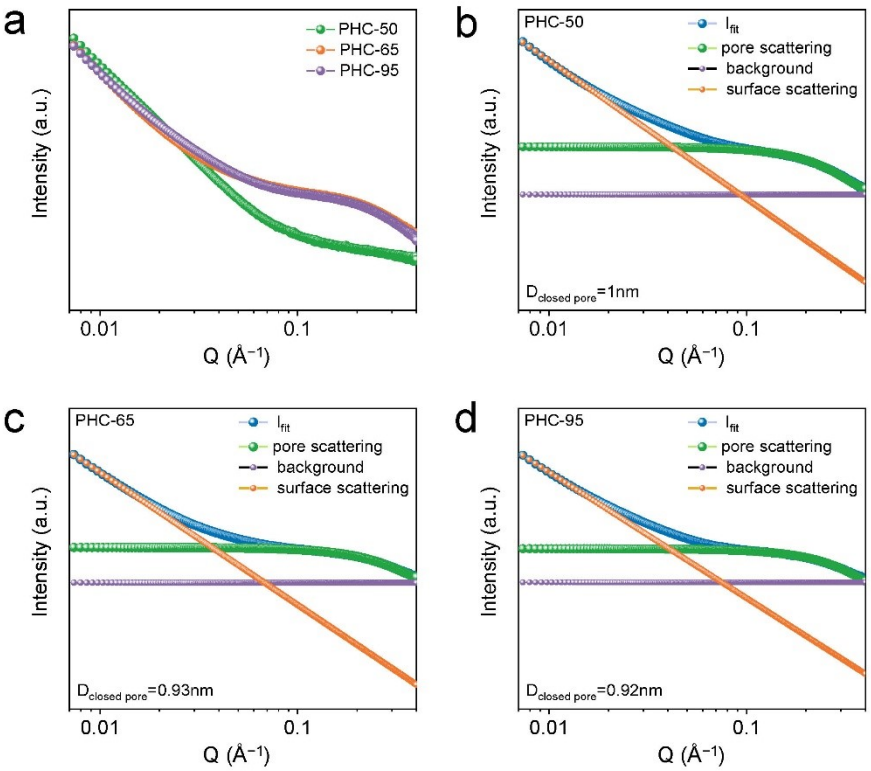

Fig. S13. (a) SAXS curves of PHC-50, PHC-65, and PHC-95. The fitted SAXS spectra of (b) PHC-50, (c) PHC-65, and (d) PHC-95.

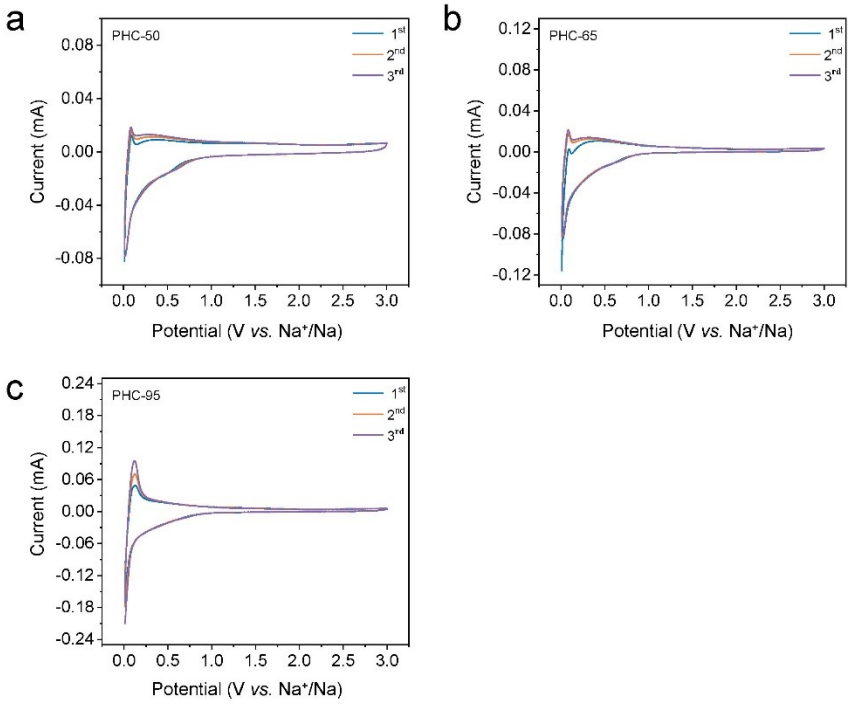

Fig. S14. CV curves for (a) PHC-50, (b) PHC-65, and (c) PHC-95 under 0.1mV s^{-1}.

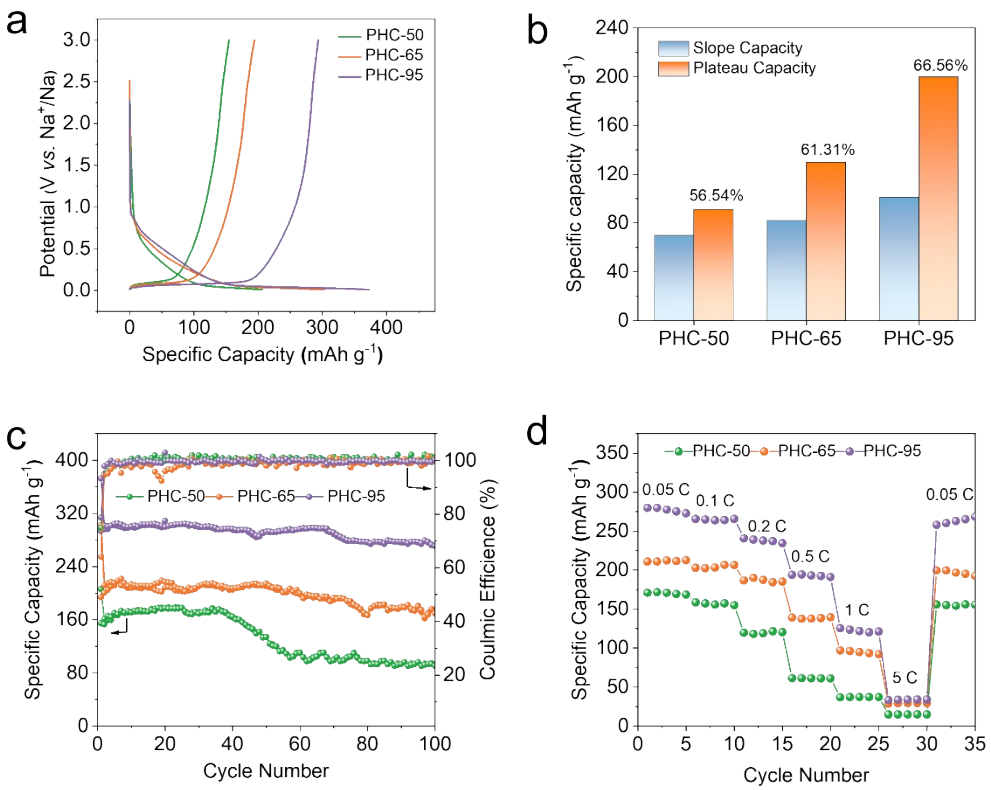

Fig. S15. (a) The initial charge/discharge curves of the half cell using PHC-50, PHC-65, and PHC-95. (b) The percentage of plateau capacity and slope capacity of the second discharging curve for PHC-50, PHC-65, and PHC-95 cells. (c) The long cycle performance and (d) rate capability of the half cell using PHC-50, PHC-65, and PHC-95.

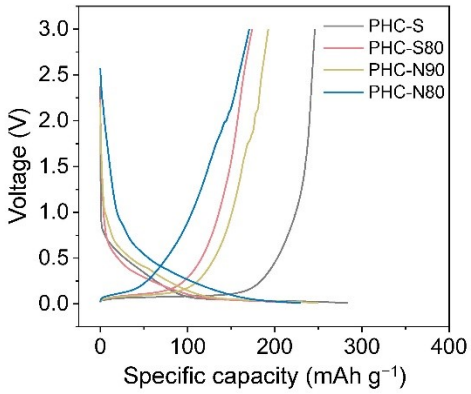

Fig. S16. Initial galvanostatic discharge/charge profiles of PHC-S, PHC-S80, PHC-N90, and PHC-N80 at 0.1 C. Two conditions were applied for sulfuric acid treatment. In the first, peony shell powder was mixed with 1 M H_2SO_4 at a solid-to-liquid ratio of 1:10 and stirred at room temperature for 6 h, then washed with distilled water until the pH reached 7, and dried at 80 ℃ for 12 h. This sample was designated PS-S. In the other group, the mixture was stirred in a water bath at 80 ℃ for 20 min, then washed to neutrality and dried, designated PS-S80. Two conditions were also used for alkali treatment. The 5 wt% NaOH solution was prepared, and peony shell powder was added at a ratio of 1:10. One batch was treated in a 90 ℃ water bath for 2 h, washed thoroughly with water until neutral, and dried at 80 ℃ for 12 h (designated PS-N90). The other group was treated at 80 ℃ for 20 min and then dried at 80 ℃ for 12 h (designated PS-N80). The carbonization process remains consistent with the previous one.

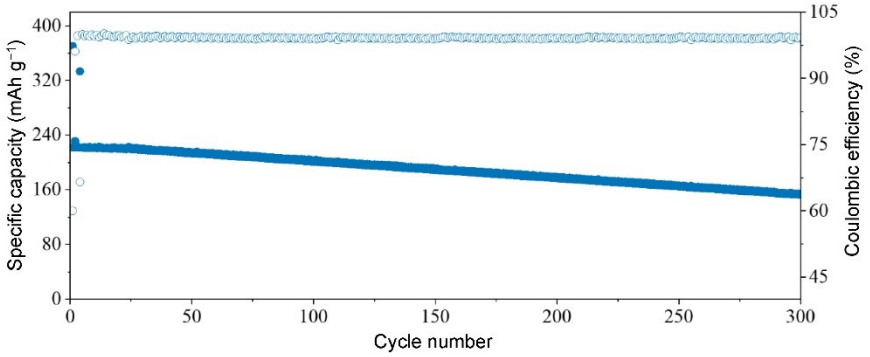

Fig. S17. Cycling performance of the half cell using PHC-80 at 1 C.

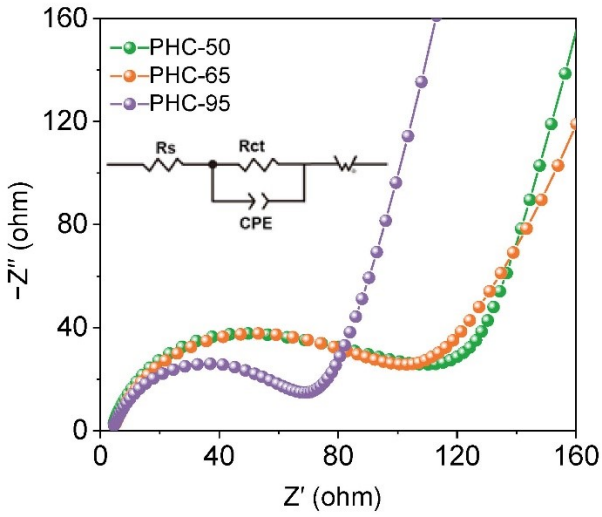

Fig. S18. The electrochemical impedance spectroscopy (EIS) curves of the half cell using PHC-50, PHC-65, and PHC-95.

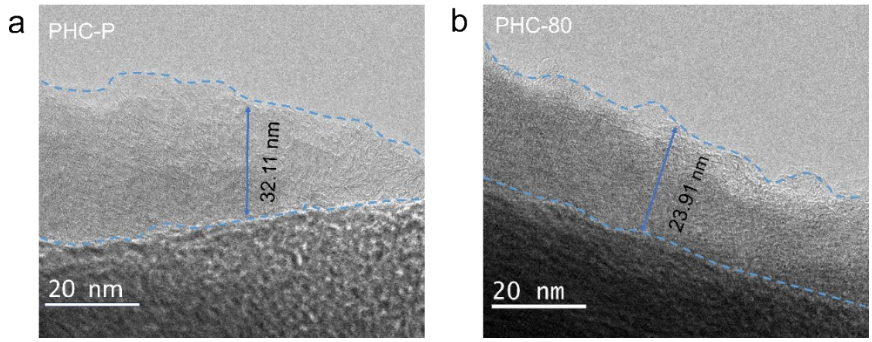

Fig. S19. HRTEM images of the SEI from (a) PHC-P and (b) PHC-80 anodes.

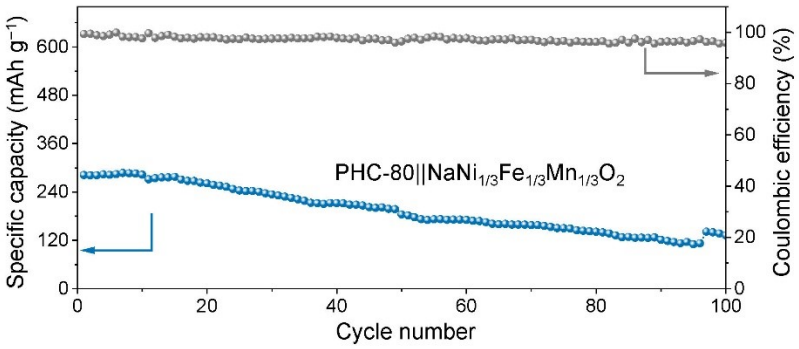

Fig. S20. Cycling performance of the full cell using PHC-80.

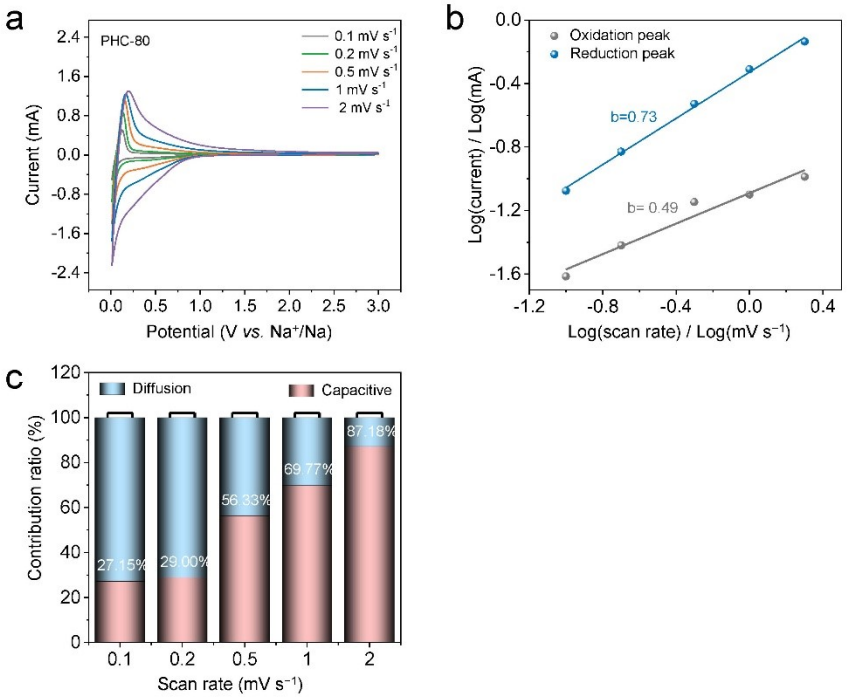

Fig. S21. (a) CV curves under different scan rates from 0.1 mV s^{-1} to 2 mV s^{-1}. (b) The relationship between lg(v) and lg(i). (c) The capacitive capacity contribution at different scan rates for PHC-80.

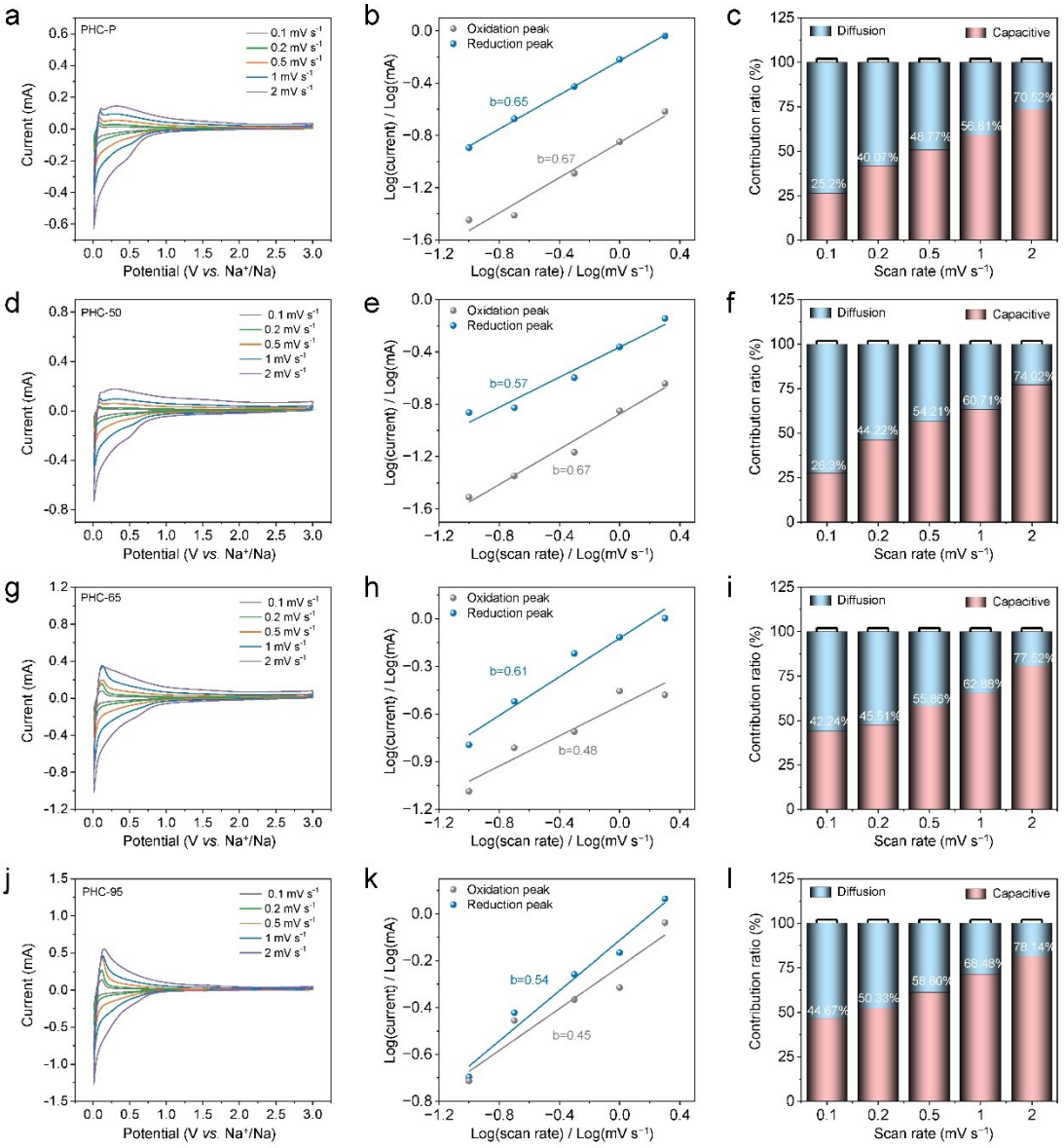

Fig. S22. CV curves and capacitive capacity contribution under different scan rates from 0.1 mV s^{-1} to 2 mV s^{-1} for (a–c) PHC-P, (d–f) PHC-50, (g–i) PHC-65, and (j–l) PHC-95.

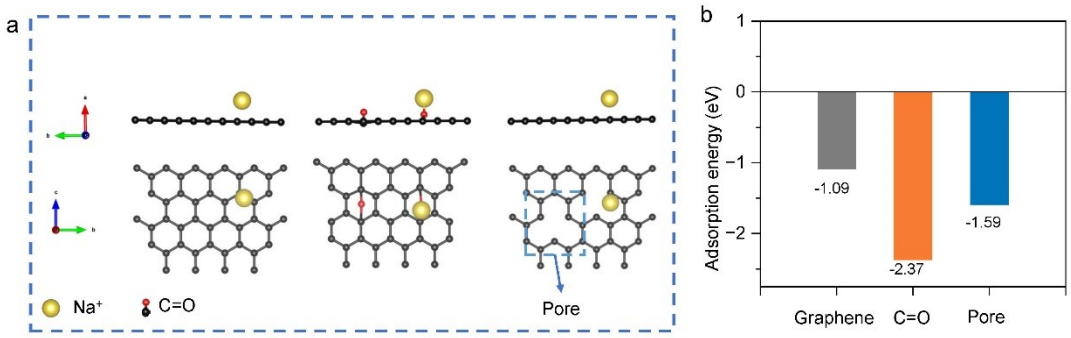

Fig. S23. (a) Schematic of Na^+ adsorption sites (monolayer). (b) Adsorption energy.

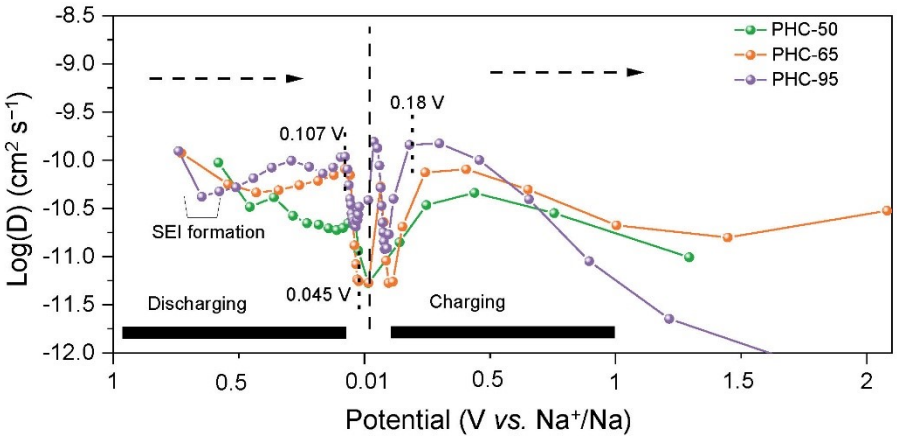

Fig. S24. Calculated Na^+ diffusion coefficients during discharge and charge of PHC-50, PHC-65, and PHC-95.

Table S1. Component analysis (wt.%) of almond shell.

Sample	cellulose	hemicellulose	lignin	ashes
PS	29.28	22.87	43.93	3.9
PS-50	35.69	18.01	42.82	3.5
PS-65	40.77	15.08	41.25	2.9
PS-80	46.75	12.44	38.60	2.2
PS-95	50.62	10.24	37.34	1.8

Table S2. Molecular weight of almond shell.

Sample	M_w	M_n	M_w/M_n
PS	185147	39731	4.66001
PS-50	147719	40760	3.62412
PS-65	123739	40760	4.06822
PS-80	118692	29944	3.96383
PS-95	102582	33515	3.06078

Table S3. Analysis parameters of the HCS from XRD and Raman spectroscopy.

	(002) peak				Disordered region			Graphite-like region			A_D/A_G
	2θ	$d_{(002)}$	$L_{c(002)}$	$L_{a(002)}$	2θ	$d_{(002)}$	Area	2θ	$d_{(002)}$	Area	
	(°)		nm		(°)	nm	(%)	(°)	nm	(%)	
PHC-P	23.797	0.373	1.99	4.07	22.067	0.403	29.29	24.6024	0.362	70.71	1.5
PHC-50	23.298	0.381	1.17	2.40	21.941	0.405	37.92	24.8255	0.359	62.08	1.6
PHC-65	23.065	0.385	1.20	2.44	21.802	0.407	45.42	24.5957	0.362	54.58	1.63
PHC-80	22.434	0.396	1.10	2.24	21.747	0.408	59.78	24.5054	0.363	40.22	2.1
PHC-95	22.700	0.392	1.20	2.44	21.887	0.406	51.87	24.6779	0.361	48.13	1.71

Table S4. The element contents of C and O in all samples.

Sample	Atomic %		Functional group %	
	C	O	C=O	C−O
PHC-P	87.88	12.12	51.95	48.05
PHC-50	89.06	10.94	49.33	50.67
PHC-65	89.79	10.21	44.19	55.81
PHC-80	90.14	9.86	36.32	63.68
PHC-95	93.76	6.24	40.26	59.74

Table S5. Pore structure analyzed from N_2 adsorption-desorption and SAXS results

Sample	N_2 adsorption-desorption			CO_2 adsorption-desorption		SAXS	
	S_{BET}	D_{pore}	V_{pore}	S_{DFT}	V_{pore}	$D_{closed\ pore}$	$V_{closed\ pore}$
	$m^2\ g^{-1}$	(nm)	$g\ cm^{-3}$	$m^2\ g^{-1}$	$g\ cm^{-3}$	(nm)	$g\ cm^{-3}$
PHC-0	145.62	2.5491	0.0928	30.7	0.01482	1.06	0.112
PHC-50	138.15	2.6008	0.0898			1.00	
PHC-65	104.12	2.5163	0.0655			0.93	
PHC-80	7.1424	3.6068	0.0064	43.865	0.01895	0.88	0.545
PHC-95	41.4	3.1936	0.0331			0.93	

Table S6. The ICE and capacity of HCS measured at a current density of 0.0279 A g^{-1}.

Sample	Reversible capacity (mAh g^{-1})	ICE (%)	2th Discharge capacity (mAh g^{-1})	Plateau capacity for 1st cycle (mAh g^{-1})	Capacity retention rate after100 cycles (%)
PHC-P	144.4	68.69	175.79	67	53.88
PHC-50	154	74.94	161.01	91	59.34
PHC-65	194	64.14	212	130	87.87
PHC-80	333	79.98	333.17	180	90.63
PHC-95	293	78.72	301.85	200	85.66

Table S7. The Na storage properties of various natural biomasses derived hard carbon.

Sources	Specific capacity (mAh g^{-1})	ICE (%)	Retention (%)/Cycle (n)/ rate (mA g^{-1})	Ref.
Cellulose	335	89	97/200/100	[1]
Oak leaves biowaste	378	84.7	97/100/30	[2]
Bamboo	320	91.4	91/300/100	[3]
Asphalt	318. 3	86.14	90/200/292	[4]
Brown coal	316.3	87.6	95/300/100	[5]
Tea	308	90	91/500/280	[6]
Rosewood lignin	326	71	85/800/500	[7]
Lignin	302	85	87/500/300	[8]
Peony shell	333	80	90/100/300	This work

References

[1] Y. Mao, Z. Yi, L. Xie, et al. *Energy Storage Mater*., 2024, 73, 103845.

[2] M. Ishaq, M. Jabeen, Y.S. He, et al. *Adv. Energy Mater*., 2025, 15, 2403142.

[3] C. Wu, Y. Yang, Y. Zhang, et al. Chou, *Angew. Chem. Int. Ed*., 2024, 63, e202406889.

[4] L.B. Wang, Z.K. Xu, P. Lin, et al. *Adv. Energy Mater.,* 2025, 15, 2403084.

[5] K. Liu, Y. Guo, B. Liu, et al. *Chin. Chem. Lett*., 2025, 111156.

[6] Q. He, H. Chen, X. Chen, et al. *Adv. Funct. Mater*., 2024, 34, 2310226.

[7] S. Zhou, Z. Tang, Z. Pan, et al. *SusMat*, 2022, 2, 357.

[8] Z. Tang, D. Jiang, Z. Fu, et al. *Small Methods*, 2024, 8, 2400509.